Applied Ocean Research 51 (2015) 293–308

Contents lists available at ScienceDirect

Applied Ocean Research

journal homepage: www.elsevier.com/locate/apor

Development of a core mathematical model for arbitrary manoeuvres of a shuttle tanker

S. Sutulo, C. Guedes Soares*

Centre for Marine Technology and Engineering (CENTEC), Instituto Superior Técnico, Universidade de Lisboa, Portugal

ARTICLE INFO

Article history:
Available online 12 February 2015

Keywords:
Ship manoeuvrability
Mathematical model
Low-speed manoeuvring
Simulation
Lateral thrusters
Tugs
Wind and current action

ABSTRACT

A 3DOF still-water manoeuvring mathematical model embracing all regimes of motion of a single-screw shuttle LNG carrier has been developed. Besides four-quadrant models for hull forces, main propeller and the rudder, the model describes also the action of a lateral thruster and of assisting tug boats. Environmental factors include constant wind and constant current. Results of off-line simulations partly compared with available trial data are given.

1. Introduction

Handling the liquefied natural gas inevitably includes processes of berthing and unberthing of an LNG carrier (shuttle tanker) to and from a floating jetty (FLNG barge). In general, such manoeuvres are considered as very complicated in seamanship practice and relatively prone to accidents, especially to ramming. Although in the majority of cases such accidents do not result in disasters or other grave consequences as the berthing manoeuvres are performed at low velocities, the very fact of handling a very dangerous and easily inflammable cargo sets augmented standards for the manoeuvring safety. The latter is supported by appropriate manoeuvring qualities of all involved craft, reasonable steering techniques and tactics, and also by extensive training of human operators with the help of computerized bridge simulators. Success of this training depends heavily on the quality of implemented core mathematical models.

A considerable number of suitable mathematical models covering the range of "normal" or moderate manoeuvres performed with the main control devices (like normal rudders) and without reversing the main propulsor can be easily found in the literature [1–4]. The parameters of these models are then to be determined from CFD computations, captive model tests or by identification from free running models experiments or full-scale trials (e.g. [5–7]).

This is much less true for the so-called low-speed models applicable in fact to the whole range of motions including such hard manoeuvres as the crash stop, crabbing and rotation on the spot. Probably, one of the first contributions being at the same time very informative belongs to [8] who supposed that all hydrodynamic forces depended on 4 dimensionless angular parameters all defined in 4 quadrants. The hull force model was based on a heuristic decomposition into: (1) ideal fluid (inertial) effects, (2) hull lifting forces, (3) hull cross-flow effects, and (4) hull resistance in longitudinal motion. The proposed 4-quadrant propeller model was based on a piecewise approximation of the thrust and torque coefficients, and, being very convenient, was used with small modifications in the present study and is described in detail in the main part of the paper. Finally, the rudder's model in the slipstream was based on a combination of tabulated rudder characteristics, on a more or less typical simplified scheme for propeller race action and, as claimed, on several ad hoc rules, omitted, however, from the publication.

Ankudinov et al. [9] noticed that quadratic (with absolute value operation when appropriate) dimensional polynomials are structurally applicable to hard manoeuvres but the regression coefficients were supposed to be estimated separately in four regions: (1) moderate drift angles ahead, (2) large drift angles ahead, (3) large drift angles astern, and (4) moderate drift angles astern. Necessity to match four separate regressions makes this approach somewhat clumsy.

Kobayashi and Asai [10] introduced two limiting values of the Froude number. Above the higher value a usual cubic dimensionless model for moderate manoeuvring was assumed applicable while below the lower value a specially devised second order quasi-polynomial dimensional regression model was used. In the intermediate region all hull forces and moments were obtained as a linear blend of the high-speed and low-speed model. The low-speed

* Corresponding author.
E-mail address: c.guedes.soares@centec.tecnico.ulisboa.pt (C. Guedes Soares).

0141-1187/$ – see front matter © 2015 Elsevier Ltd. All rights reserved.
http://dx.doi.org/10.1016/j.apor.2015.01.008

model was used also in astern motion but with different regression coefficients.

Khattab [11] also assumed that different physical phenomena associated with the lift (side force) with and without separation and with the cross-flow drag dominate for different intervals of the drift angle. Full regressions for the sway force and the yaw moment are subdivided into three single-variable parts (depending on the drift angle and two dimensionless yaw rate parameters) valid, however in the whole range of manoeuvres. The regression coefficients were chosen in such a way that the regressions match asymptotically some earlier devised polynomial model while coefficients corresponding, say, to crabbing were estimated with the cross-flow drag theory.

It can be also noticed that later publications avoided giving more or less detailed descriptions of mathematical models especially four-quadrant ones [12]. In fact, practically all ship handling simulators imply core models exactly of the extended type [13]. But these models are typically considered as proprietary and, as far as it could be detected or suspected, are more often than not based on certain tricks and quick "at hand" solutions maybe indeed not deserving advertisement.

In the present paper, an attempt is undertaken to develop a comprehensive unified versatile mathematical model suitable for all types of manoeuvres in still water i.e. no wave excitation is considered. Special attention was paid to the model being relatively consistent from the viewpoint of basic principles [14]. Although the resulting model is similar in many respects to other published models and is thus based on some synthesis, it contains also a number of novelties and improvements not encountered in the literature. All of them are described in detail and it is believed that these elements could become useful in other applications.

The model was applied to a shuttle LNG carrier *Galea*, for which some trial data were available. Mostly, these full-scale results were used for comparisons with the predicted behaviour of the ship. Contrary to normal practice followed by developers of ship handling simulators [15] the model was not subject to extensive adjustments except for lateral thruster action commented in the main text body. Computer implementation of the developed model was performed as series of extensions of the object-oriented multi-model code developed earlier by the authors [16].

Finally, it is worthwhile to note that the popular term "low-speed manoeuvring" is somewhat misleading and not very exact. In fact, every time it is used it goes about the hard manoeuvres mentioned above. Indeed, such manoeuvres can only be performed at slow speed as otherwise power requirements would greatly exceed the available from the main engine. On the other hand, normal manoeuvres reachable with constant engine settings and with the normal rudder can be executed at *any* speed, at least with the turbine-driven vessel which, contrary to diesel engines, does not possess a stall (idle) rotation frequency. For moderate and low values of the Froude number, all reasonable manoeuvring characteristics remain practically independent of speed and, when properly rescaled in time, the behaviour of the ship must be independent of the approach speed. However, there is a general belief that any ship is worse controllable in low speed [17] and that is why auxiliary steering devices are indispensable. There are two possible causes of this paradox or rather misunderstanding. First, although the response to control actions remains adequate, it becomes really slower in the dimensional time while the human operator's own time scale remains the same and the subjective perception tells about worse controllability. The second circumstance is the increased sensitivity to external factors, such as wind and current, because rudder steering forces are approximately proportional to the square of the ship speed. It is, however, meaningless to discuss the loss of controllability at low speed if the level of external influence is not specified.

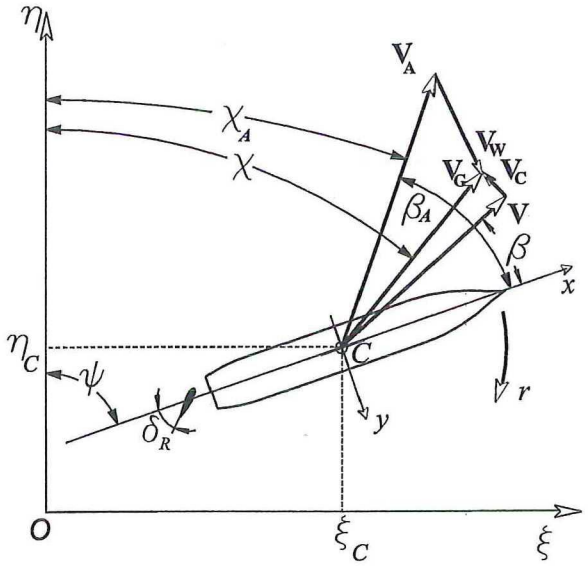

Fig. 1. Frames of reference.

2. General structure of ship manoeuvring model

2.1. Frames of reference and kinematic parameters

The used frames of reference are shown in Fig. 1 in the horizontal plane view: the Earth-fixed frame $O\xi\eta\zeta$ with the axis $O\zeta$ directed vertically downwards is used to describe the ship trajectory and to define the steady wind characterized by the wind speed $\mathbf{V}_W$ or by its magnitude $V_W = |\mathbf{V}_W|$ and by the wind angle X_W. Similarly, the steady uniform current velocity is $\mathbf{V}_C$ also defined by the couple (V_c, χ_c). The origin O is placed on the undisturbed free surface and its location in the horizontal plane, as well as the orientation of the two horizontal axes can be arbitrary. As a rule, they are chosen from convenience considerations. For instance, if some standard manoeuvre as the turning circle is considered, it is natural to match the origin with the ship's location at the start of the manoeuvre i.e. when the corresponding order is given. In the case of berthing/unberthing, the Earth-fixed frame typically matches the moored position of the ship.

The ship motion is described by the ground velocity vector $\mathbf{V}_G$ and by the angular velocity vector $\boldsymbol{\Omega}$. Introducing the air ship velocity vector $\mathbf{V}_A$ and the ship velocity vector $\mathbf{V}$ (magnitude of the latter is the ship's log speed) it is easy to establish the following relations:

$$\begin{aligned} &\mathbf{V}_G = \mathbf{V}_A + \mathbf{V}_W, \\ &\mathbf{V}_G = \mathbf{V} + \mathbf{V}_c. \end{aligned} \tag{1}$$

It follows from these relations that

$$\begin{aligned} &\mathbf{V}_A + \mathbf{V}_W = \mathbf{V} + \mathbf{V}_c, \\ &\mathbf{V} = \mathbf{V}_G - \mathbf{V}_c, \\ &\mathbf{V}_A = \mathbf{V}_G - \mathbf{V}_W = \mathbf{V} + \mathbf{V}_c - \mathbf{V}_W. \end{aligned} \tag{2}$$

The wind and current velocities can be also represented through their projections on the Earth axes (the vertical components are supposed to be zero):

$$\begin{aligned} &V_{w\xi} = V_W \cos\chi_W; \quad V_{w\eta} = V_W \sin\chi_W, \\ &V_{c\xi} = V_c \cos\chi_c; \quad V_{c\eta} = V_c \sin\chi_c. \end{aligned} \tag{3}$$

As usual, the body axes $Cxyz$ are introduced with the origin C lying at any point in the centreplane although usually preferred is either the centre of mass or the point belonging also to the midship plane and to the equilibrium waterplane. The position of the body

axes with respect to the Earth frame is described by the advance ξ_C, transfer η_C, submergence ζ_C, heading angle ψ, pitch angle θ and roll angle φ. Projections of the velocity $\mathbf{V}$ onto the body axes x, y, z are denoted as u, v, w and called velocities of surge, sway, and heave respectively and those of the angular velocity $\boldsymbol{\Omega}$ are p, q, and r and called velocities of roll, pitch and yaw. The subscripts w, c, G, A can be added to any velocity to refer to the corresponding component.

It follows from Eqs. (1)–(3) that

$$u_G = u + u_c; \quad v_G = v + v_c; \\ u_A = u_G - u_w; \quad v_A = v_G - v_w. \tag{5}$$

The formulae above are very important as they determine peculiarities of the ship motion in presence of wind and current. The wind and current velocities, which are present there, are:

$$u_c = \; V_{c\xi}\cos\psi + V_{c\eta}\sin\psi, \\ v_c = -V_{c\xi}\sin\psi + V_{c\eta}\cos\psi, \\ u_w = \; V_{w\xi}\cos\psi + V_{w\eta}\sin\psi, \\ v_w = -V_{w\xi}\sin\psi + V_{w\eta}\cos\psi. \tag{6}$$

The main state variables of the manoeuvring ship will be ξ_C, η_C, ψ, r, and u, v although each of the latter two can be substituted with a corresponding ground or air velocity. The following auxiliary variables can often become useful:

- the dimensionless velocities of sway and yaw

$$v' = \frac{v}{V}, \quad r' = \frac{rL}{V}, \tag{7}$$

where $V = |\mathbf{V}|$ and L is the ship's reference length;

- the drift angle (with respect to water)

$$\beta = \begin{cases} -\operatorname{asin} v' & \text{at} \quad u \geq 0, \\ -\pi \operatorname{sign} v + \operatorname{asin} v' & \text{at} \quad u < 0; \end{cases} \tag{8}$$

- the air drift angle

$$\beta_A = \begin{cases} -\operatorname{asin} v'_A & \text{at} \quad u_A \geq 0, \\ -\pi \operatorname{sign} v_A + \operatorname{asin} v'_A & \text{at} \quad u_A < 0, \end{cases} \tag{9}$$

where $v'_A = v_A/V_A$ and $V_A = |\mathbf{V_A}|$ is the ship's air speed equal to the relative wind speed as measured on the ship;

- the course angle υ (with respect to water)

$$\upsilon = \psi - \beta; \tag{10}$$

- the course (angle) χ over the ground

$$\chi = \begin{cases} \operatorname{asin}\frac{\dot\eta_C}{\dot\xi_C} & \text{at} \quad \dot\xi_C > 0, \quad \dot\eta_C > 0, \\ \pi + \operatorname{asin}\frac{\dot\eta_C}{\dot\xi_C} & \text{at} \quad \dot\xi_C < 0, \\ 2\pi + \operatorname{asin}\frac{\dot\eta_C}{\dot\xi_C} & \text{at} \quad \dot\xi_C > 0, \quad \dot\eta_C < 0. \end{cases} \tag{11}$$

The usual dimensionless velocities v' and r' are not convenient for hard manoeuvres as they tend to infinity as the ship speed tends to zero. The drift angle is used instead of the dimensionless velocity of sway and the following generalized dimensionless velocity of yaw can be introduced:

$$r'' = \frac{rL}{\sqrt{V^2 + r^2L^2}} = \frac{r'}{\sqrt{1 + r'^2}} \tag{12}$$

It is clear that $r'' \in [-1, 1]$ remaining always finite.

The plane $\beta - r''$ (Fig. 2) can be used to represent domains of arbitrary (all imaginable) manoeuvres (the large rectangle), moderate manoeuvres (the smaller hatched rectangle), and weak manoeuvres (the smallest filled rectangle; weak manoeuvres are typically course keeping and small course changes). Of course, the boundaries separating the domains from each other are fuzzy and traced basing on rather arbitrary expert estimates.

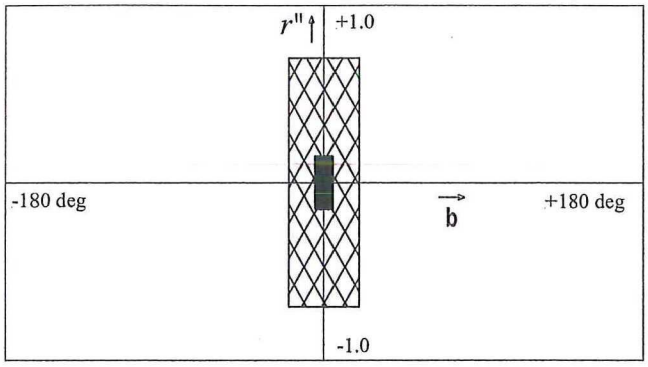

Fig. 2. Sketch of manoeuvring domains.

2.2. Equations of motion

In low-speed manoeuvring, effects related to the vertical planes are negligible and it can be assumed that the manoeuvring motion is only performed in the horizontal plane. The kinematic differential equations linking the ship's position in the Earth axes with the velocities projections are then

$$\dot\xi_C = u_G\cos\psi - v_G\sin\psi, \\ \dot\eta_C = u_G\sin\psi + v_G\cos\psi, \\ \dot\psi = r. \tag{13}$$

The dynamic equations of motion of the ship as a rigid body are:

$$(m + \mu_{11})\dot u - mvr - mx_Gr^2 = X_H + X_P + X_R + X_A + X_Q, \\ (m + \mu_{22})\dot v + (mx_G + \mu_{26})\dot r + mur = Y_H + Y_P + Y_R + Y_T + Y_A + Y_Q, \\ (mx_G + \mu_{26})\dot v + (I_{zz} + \mu_{66})\dot r + mx_Gur = N_H + N_P + N_R + N_T + N_A + N_Q, \tag{14}$$

where m is the mass of the ship; μ_{ij} are the added masses, x_G, y_G are the centre-of-mass coordinates; I_{zz} is the moment of inertia in yaw; X, Y, N are the forces and moments of surge, sway, and yaw respectively and each of these components is divided into subcomponents described by the following subscripts: H—the hull hydrodynamic forces, P—the propeller forces, R—the rudder forces, T—the thruster forces, A—the aerodynamic forces, Q—forces from the tugs.

3. Hydrodynamic hull forces

The hydrodynamic forces on the hull are described using the method proposed by Sutulo [18] which, in its present implementation, represents a continuation of the standard Inoue model onto the domain of arbitrary manoeuvres. According to this method, the hull sway force and yaw moment are represented as:

$$X_H = X''\frac{\rho}{2}(V^2 + L^2r^2)LT, \\ Y_H = Y''\frac{\rho}{2}(V^2 + L^2r^2)LT, \\ N_H = N''\frac{\rho}{2}(V^2 + L^2r^2)L^2T, \tag{15}$$

where X'', Y'', N'' are the generalized force and moment coefficients.

As to the surge force, it turned out that the most convenient approach is to transform the surge force model suggested by Inoue et al. [19]. Besides moving from the dimensional to the dimensionless form, the structure was corrected in such a way that the surge

force vanishes when the ship is rotating on the spot independently of the drift angle (strictly speaking, there will be some nonzero surge force for a ship without midship symmetry but obviously it will not be significant and in case of absence of experimental data should be better zeroed). Then, the generalized surge force coefficient is

$$X''_H = -\frac{2R_T(u)r_{AS}(u)}{\rho V^2 LT}\cos\beta|\cos\beta|(1-r''^2) - \frac{2C_m\mu_{22}}{\rho L^2 T}\sin\beta\, r''\sqrt{1-r''^2} \tag{16}$$

where $R_T(u)$ is the total resistance curve as function of the surge velocity and defined for both positive and negative argument, r_{AS} is the astern correction coefficient, $C_m \approx 0.625$ is the correction factor [19].

As the drag curve in astern motion is usually unavailable and not supported with standard resistance prediction methods [20], it was assumed here to be odd i.e. $R_T(-u) = -R_T(u)$. However, as usually the hull is optimized for the ahead motion, the correction coefficient r_{AS} is assumed to be 1.15 at $u<0$ and 1.0 otherwise.

The dimensionless sway and yaw coefficients can be modelled as follows:

$$Y''(\beta, r'') = c_{y0}r'' + c_{y1}\sin\beta\sin\pi r''\,\mathrm{sign}\,r'' + c_{y2}\sin\beta\cos\frac{\pi}{2}r'' + c_{y3}\sin 2\beta\cos\frac{\pi}{2}r'' + c_{y4}\cos\beta\sin\pi r'' + c_{y5}\cos 2\beta\sin\pi r'' + c_{y6}\cos\beta\left(\cos\frac{\pi}{2}r'' - \cos\frac{3\pi}{2}r''\right)\mathrm{sign}\,r'' + c_{y7}(\cos 2\beta - \cos 4\beta)\cos\frac{\pi}{2}r''\,\mathrm{sign}\,\beta + c_{y8}\sin 3\beta\cos\frac{\pi}{2}r''; \tag{17}$$

$$N''(\beta, r'') = c_{n0}r'' + c_{n1}\sin 2\beta\cos\frac{\pi}{2}r'' + c_{n2}\sin\beta\cos\frac{\pi}{2}r'' + c_{n3}\cos 2\beta\sin\pi r'' + c_{n4}\cos\beta\sin\pi r'' + c_{n5}(\cos 2\beta - \cos 4\beta)\sin\pi r'' + c_{n6}\cos\beta(\cos\beta - \cos 3\beta)\,\mathrm{sign}\,r'' + c_{n7}\sin 2\beta\left(\cos\frac{\pi}{2}r'' - \cos\frac{3\pi}{2}r''\right) + c_{n8}\sin\beta\left(\cos\frac{\pi}{2}r'' - \cos\frac{3\pi}{2}r''\right) + c_{n9}\sin 2\beta\left(\cos\frac{\pi}{2}r'' - \cos\frac{3\pi}{2}r''\right)\mathrm{sign}\,r''. \tag{18}$$

The regression coefficients $c_{y,ni}$ in (17) and (18) would be best determined after captive-model tests carried out for each particular hull in the whole range of the drift angle and dimensionless rate of yaw. However, such experimental data are obtained rarely and, as a bypass solution, these coefficients can be chosen to provide asymptotic equivalence to polynomial models devised for moderate manoeuvres. These polynomial models can be developed specifically for the given hull or borrowed from some database method, like that by Inoue et al. [19]. These models are normally written in terms of primed variables v', r' but can be re-written in terms of β and r':

$$\begin{aligned} Y''(\beta, r') &= -Y'_v\sin\beta + Y'_r r' - Y'_{v|v|}\sin\beta|\sin\beta| - Y'_{v|r|}\sin\beta|r'| + Y'_{r|r|}r'|r'|,\\ N''(\beta, r') &= -N'_v\sin\beta + N'_r r' + N'_{vvr}\sin^2\beta\, r' - (N'_{vrr} - N'_v)\sin\beta\, r'^2 + N'_{r|r|}r'|r'|, \end{aligned} \tag{19}$$

where the coefficients $Y'_v, \ldots, N'_{r|r|}$ are functions of the hull's particulars and trim and are estimated according to Inoue et al. [21].

Then, the regressions (17) and (18) can be re-written in terms of the same variables as (19) using the relation $r'' \approx r' - \frac{1}{2}r'^3$ and then asymptotically matched to (19). Their structure, which may seem at first sight not quite natural and evident, was chosen to make this matching possible. As result, the following relations can be established:

$$\begin{aligned} &c_{y0} = Y''_0;\quad c_{y1} = -\frac{1}{\pi}Y'_{vr};\quad c_{y2} = -\frac{1}{2}[Y'_v(\tau) + Y'_v(-\tau)] + \frac{3}{4}Y''_*;\\ &c_{y3} = -\frac{1}{4}[Y'_v(\tau) - Y'_v(-\tau)];\quad c_{y4} = \frac{1}{2\pi}[Y'_r(\tau) + Y'_r(-\tau)];\\ &c_{y5} = \frac{1}{2\pi}[Y'_r(\tau) - Y'_r(-\tau) - 2Y''_0];\quad c_{y6} = \frac{1}{\pi^2}Y'_{rr};\quad c_{y7} = -\frac{1}{6}Y'_{vv};\\ &c_{y8} = -\frac{1}{4}Y''_*;\quad Y''_* = Y''_{90} + \frac{1}{2}[Y'_v(\tau) + Y'_v(-\tau)] - \frac{1}{3}Y'_{vv}, \end{aligned} \tag{20}$$

$$\begin{aligned} &c_{n0} = N''_0;\quad c_{n1} = -\frac{1}{4}[N'_v(\tau) + N'_v(-\tau)];\quad c_{n2} = -\frac{1}{2}[N'_v(\tau) + N'_v(-\tau)];\\ &c_{n3} = -\frac{1}{2\pi}[N'_r(\tau) + N'_r(-\tau)] - 2N''_0;\quad c_{n4} = \frac{1}{2\pi}[N'_r(\tau) - N'_r(-\tau)];\\ &c_{n5} = \frac{1}{6\pi}[N'_{vvr} + N'_r(\tau) + N'_r(-\tau) - 2N''_0];\quad c_{n6} = \frac{1}{16\pi}[N'_r(\tau) - N'_r(-\tau)];\\ &c_{n7} = -\frac{1}{2\pi^2}N'_{vrr} + \left(\frac{1}{4\pi^2} - \frac{1}{32}\right)[N'_v(\tau) + N'_v(-\tau)];\\ &c_{n8} = \left(\frac{1}{2\pi^2} - \frac{1}{16}\right)[N'_v(\tau) - N'_v(-\tau)];\quad c_{n9} = -\frac{1}{\pi^2}N'_{rr}, \end{aligned} \tag{21}$$

where τ is the trim, positive by the stern and nondimensionalized by the mean draught; Y''_0 and N''_0 are the generalized sway force and yaw moment coefficients determined for the hull rotating on the spot, and Y''_{90} is the generalized yaw moment coefficient corresponding to the pure lateral motion i.e. to the crabbing without rotation. If these data are absent, which is typical, they can be estimated using the method from (Voytkunsky, 1985) or estimated with the cross-flow drag technique. Because of the absence of data related to the astern motion with moderate drift angles, it was additionally assumed that the hull is symmetric with respect to the midship plane. At the same time, the fact that a trim by the stern will act as a trim by the bow in astern motion is accounted for.

Finally, it must be noted that the original mathematical model by Inoue et al. [19,21] is 4DOF involving also the roll equation and dependence of the yaw moment on the instantaneous roll angle. The back influence of the roll may become significant for relatively fast vessels. The ship considered in the present study is marginal in this respect and using a 4DOF model could be desirable. However, as the investigation was here more concentrated on the low-speed manoeuvring and creation of uniformly valid regressions including roll effects is problematic and certainly not straightforward, the choice was made in favour of a 3DOF manoeuvring model which finally proved quite adequate in the present case.

4. Propeller forces

The propeller's longitudinal force $X_P = T_e$, where T_e is the effective thrust which is supposed to be positive when the propeller is

running ahead and is negative when working astern. The effective thrust is obtained from the open-water thrust T as

$$T_e = T(1 - t_P), \tag{22}$$

where t_P is the thrust deduction fraction.

For any given fixed-pitch propeller, the thrust will depend on the current rotation frequency (rps) n, which is assumed positive in ahead rotation and on the instantaneous propeller advance velocity $u_{PA} = u(1 - w_P)$, where w_P is the propeller wake fraction. To simulate arbitrary manoeuvres, the propeller open-water characteristics must be defined in four quadrants i.e. for any signs of n and u_{PA}. However, as studies of propeller hydrodynamics were mainly driven by interests of propulsion calculations and propeller design, relatively full sets of data corresponding to various propeller series and for full range of the number of blades, pitch and disc ratio, are only available for the first quadrant i.e. when $u_{PA} > 0$, $n > 0$ [22]. As to 4-quadrant characteristics, systematic data and approximations [23] were apparently obtained for only the B4.70 propeller while only selected pitch ratios were covered for propellers with other number of blades and different values of the disc ratio.

In the present study, an approximate alternative solution based on re-scaling of the 4-quadrant model for a unique base propeller model is proposed. The possibility of such approach follows from the fact that nearly all propeller thrust and torque coefficient curves are approximately equidistant in the first quadrant and can be transformed each to other re-scaling the axes. In fact, this operation is desirable even if the actual propeller's data are available as all methods for predicting the ship resistance, thrust and propeller–hull interaction are approximate and must be adjusted to reproduce the actual propulsion point. The adjustment procedure depends on the available input data and in a rather typical case, when the design rps n_d, the design speed V_d, the corresponding torque Q_{Pd} and the propeller diameter D_P are specified, the adjustment is performed as follows:

1. The design drag $R_{Td}(V_d)$, the straight run wake fraction w_{P0} and the thrust deduction coefficient t_{P0} are estimated using some appropriate method [20]. The design advance ratio is then $J_d = V_d(1 - w_{P0})/(n_d D_P)$.
2. The advance correction factor k_J is computed assuming that the propeller works in the design conditions at maximum efficiency (in most cases, the propellers are designed meaning this target): $k_J = J_{opt}/J_d$, where J_{opt} is the value of the advance ratio corresponding to the reference screw propeller.
3. The thrust and torque correction factors k_T and k_Q are defined as follows:

$$k_T = \frac{R_{Td}}{T_{opt}(n_d, k_J V_d)(1 - t_{P0})}, \quad k_Q = \frac{Q_d}{Q_{opt}(n_d, k_J V_d)} \tag{23}$$

where T_{opt} and Q_{opt} are the values of the thrust and torque produced by the propeller model at the shifted design propulsion point, which is optimal for the reference propeller.

After the adjustment is completed, the effective thrust and torque are continuously computed as

$$T_e = (1 - t_P)k_T \frac{\rho}{2} A_d C_T(\gamma_B) V_B^2,$$
$$Q = k_Q \frac{\rho}{2} A_d D_P C_Q(\gamma_B) V_B^2, \tag{24}$$

where t_P is the current value of the trust deduction coefficient; $A_d = \pi D_P^2/4$ is the propeller disc area; γ_B is the effective blade advance angle, and V_B is the effective total blade velocity. According to Oltmann and Sharma [8] the generalized thrust and torque coefficients are

$$C_{T,Q} = \begin{cases} C^0_{T,Q} + C^c_{T,Q}\cos\gamma_B + C^s_{T,Q}\sin\gamma_B & \text{at } \cos\gamma_B \geq 0.9336 \\ C^{cc}_{T,Q}\cos\gamma_B\left|\cos\gamma_B\right| + C^{ss}_{T,Q}\sin\gamma_B\left|\sin\gamma_B\right| & \text{otherwise} \end{cases} \tag{25}$$

where the coefficients $C^0_{T,Q}, \ldots, C^{ss}_{T,Q}$ are only defined for the a 5-bladed propeller with the pitch ratio 0.745 and the expanded area ratio 0.6; $\sin\gamma_B = \frac{k_J u_{PA}}{V_B}$, $\cos\gamma_B = \frac{V_{CP}}{V_B}$, and $V_{CP} = 0.7\pi n D_P$, $V_B = \sqrt{(k_J u_{PA})^2 + V_{CP}^2}$.

The wake fraction coefficient w_P according to Inoue et al. [19] can be approximated by

$$w_P = w_{P0} e^{-4\beta_P^2} \tag{26}$$

where β_P is the local geometric (i.e. without the hull's influence) sidewash angle. Although the approximation (26) was primarily devised for only moderate manoeuvres, it is evident that it will give reasonable estimate for all $\beta_P \in [-\pi, \pi]$.

The rotating propeller will, in general, produce also the sway force Y_P and the yaw moment N_P. These forces are, however, insignificant on moderate-speed vessels except for the case when the propeller is working astern. In this case, the so-called Hovgaard force will appear due to the influence of the tangential induced velocities in the slipstream of a heavily loaded propeller. The Hovgaard force must be accounted for when the ship is stopping and backing. Direction of the Hovgaard force depends on the direction of rotation of the propeller.

In the described model the Hovgaard force is modelled using a very simple method suggested in [24] and defining this force as a constant fraction of the thrust: $Y_P = \kappa_H T$, where the coefficient depends on the configuration of the afterbody, varies mainly from 0.4 to 0.8 but must be adjusted after trials whenever possible. Then, the yaw moment will be $N_P = Y_P x_{PH}$, where the effective abscissa x_{PH}, according to Brix' data varies from $0.78x_P$ to $0.94x_P$. Obviously, this model for the Hovgaard effect is somewhat simplistic as Anissimova and Sobolev [25] demonstrated that dependence of the force and moment on the advance ratio is in fact rather complicated. Unfortunately, contrary to what was claimed by Ambrosovsky and Katz [26], attempted implementation of the formulae proposed in the cited publication did not result in reasonable response of the ship.

5. Rudder forces

5.1. General remarks

Descriptions of practical mathematical models of rudder forces valid in moderate manoeuvring are abundant in the literature. All of them presume that the flow attacks the rudder more or less from the leading edge and the attack angles do not exceed the stall angle. Moreover, although typical modern rudders have a small aspect ratio λ_R practically never exceeding 2.0 which results in a sensitive nonlinearity of their lift curve, this circumstance is often neglected and the rudder's characteristic is linearized [19,27]. Influence of the slipstream is primarily accounted for on the basis of the actuator disc theory but many empiric corrections and, often, inconvenient structure of the formulae for the propeller influence on the rudder inflow velocity and sidewash angle make difficult their generalization to arbitrary manoeuvres. The model proposed in the present paper is free of such problems and remains valid in any situation although it is not uniformly accurate. While in moderate manoeuvring it could be validated against multiple more or less acknowledged models, the direct validation was too difficult in such situations as large attack angles of the rudder, especially

when the flow comes from the trailing edge. Assimilation, analysis and generalization of various ideas and partial models suggested by other specialists served as important assets in developing the model described below. However, special attention was given to contributions by Söding [28,29], Oltmann and Sharma [8], and Kose [30].

5.2. Basic assumptions

All engineering methods for estimating contribution of the rudder in manoeuvring motion are based on more or less natural, though not very rigorous assumptions. The following assumptions were taken here:

1. The total rudder area $A_R = A_{R0} + A_{RP}$ is composed of two parts: A_{R0} is the area outside the slipstream while A_{RP} is the area inside the slipstream. If there is no direct data about these areas, it is usually assumed that

$$A_{RP} = \frac{h_{RP}}{h_R} A_R, \tag{27}$$

   where h_{RP} is the height of the rudder's part washed by the slipstream.
2. The slipstream jet is supposed to be circular cylindrical from the rudder's leading to trailing edge.
3. Values of the rudder force coefficients (lift coefficient C_{RL}, drag coefficient C_{RD}, normal force coefficient C_{RN}, and the tangential force coefficient C_{RT}) are the same for its parts outside and inside the slipstream. In addition, it is assumed that the tangential force can always be neglected.
4. The flow around the rudder is supposed to be uniform and homogeneous within each of the parts outside and inside the propeller race. The velocity of the rudder with respect to water is $\mathbf{V}_R$ and $\mathbf{V}_{RP}$ in each area respectively and the corresponding attack angles are α_R and α_{RP}. Each attack angle is changing within the interval $[-\pi, \pi]$.

5.3. Representation of forces on the rudder

Depending on whether the force acting on the rudder is analyzed in the inflow-velocity axes or in the blade-fixed frame, considered are either the lift L and the drag D or the normal N and the tangential T force components. The latter approach has certain advantages. The plot in Fig. 3 was recalculated from the lift and drag data obtained for a non-symmetric 5% profile in circular wind tunnel tests [31] and clearly shows that the tangential force can be practically always neglected.

Assuming that the rudder normal force N is positive when directed to the rudder's portside, the rudder-originated surge force X_R and sway force Y_R will be:

$$\begin{aligned} X_R &= -N \sin \delta_R, \\ Y_R &= -(1 + a_H) N \cos \delta_R, \end{aligned} \tag{28}$$

where δ_R is the rudder deflection angle which is positive when the rudder is deflected to the starboard, and a_H is the rudder–hull interaction fraction. The rudder yaw moment is then

$$N_R = Y_R x_{RH}, \tag{29}$$

where x_{RH} is the rudder's hydrodynamic abscissa accounting for the shift of the sway force application point due to realization of its part on the hull. Inoue et al. [19] recommend $x_{RH} = x_R$, where x_R is the actual abscissa of the rudder's stock, and $a_H = 0.633 C_B - 0.153$. According to Söding [28]

$$\begin{aligned} x_{RH} &= x_R + \frac{0.3T}{e_R/T + 0.46}, \\ a_H &= \frac{1}{1 + (4.9 e_R/T + 3 b_R/T)^2}, \end{aligned} \tag{30}$$

where e_R is the average gap between the rudder's leading edge.

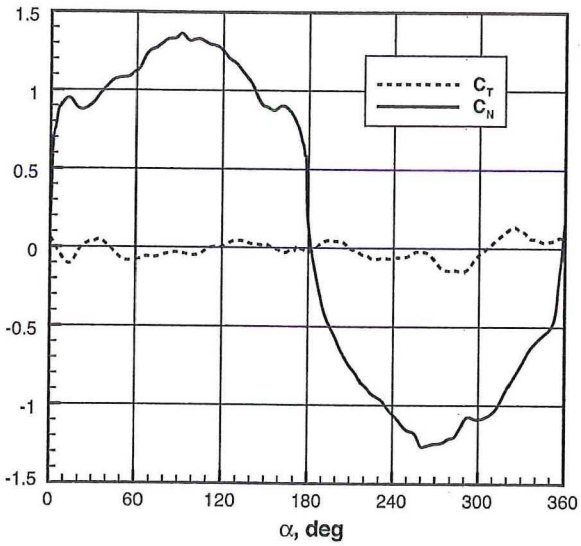

Fig. 3. Wind tunnel data for tangential and normal force coefficients C_T, C_N as function of the attack angle.

According to the assumptions (1)–(4) formulated above, the rudder normal force can be represented as

$$N = C_N(\alpha_R) \frac{\rho V_R^2}{2} A_{R0} + C_N(\alpha_{RP}) k_d \frac{\rho V_{RP}^2}{2} A_{RP} \tag{31}$$

where $k_d < 1$ is the jet deflection reduction factor specified later.

The normal force coefficient dependency $C_N(\alpha)$ must be defined in different regimes:

- The pre-stall regime when the leading edge is moving ahead with respect to the water. If the stall angle in ahead motion is α_S, then at $|\alpha| \le \alpha_s$ the response will be defined by [1]:

$$C_{N0}(\alpha) = C_{DR}(\alpha) \sin \alpha + C_{LR}(\alpha) \cos \alpha. \tag{32}$$

  Here:

$$\begin{aligned} C_{LR}(\alpha) &= (C_{L1}^{\alpha} + C_{L2}^{\alpha} |\alpha|)\, \alpha, \\ C_{DR}(\alpha) &= C_{DR0} + C_{DR1} \quad C_{LR}^2(\alpha), \end{aligned} \tag{33}$$

  where various coefficients are:

$$C_{L1}^{\alpha} = \frac{C_{L\infty}^{\alpha} \lambda_R}{\cos \Lambda \sqrt{\lambda_R^2 / \cos^4 \Lambda + 4} + 2 a_{\infty}}, \tag{34}$$

  – the rudder lift gradient,

$$C_{L\infty}^{\alpha} = 2\pi a_{\infty}, \tag{35}$$

  – the infinite aspect ratio lift gradient, and $a_{\infty} \approx 0.9$ is the viscosity correction factor. Λ is the sweep angle close to zero in most cases. Then,

$$C_{L2}^{\alpha} = C_D / \lambda_R \tag{36}$$

and

$$C_D = \begin{cases} 0.1 + 0.7b' & \text{for faired tip,} \\ 0.1 + 1.6b' & \text{for squared tip;} \end{cases} \tag{37}$$

$b' = b_t/b_r$ is the rudder taper ratio; b_t is the tip chord, and b_r is the root chord. C_{DR0} is the profile drag coefficient (0.0065 for the NACA-0015 profile), and

$$C_{DR1} = \frac{1}{\pi a_\infty \lambda_R}. \tag{38}$$

In astern motion i.e. when the rudder is moving with its trailing edge forward, the flow will be not stalled when $|\alpha| > \pi - \alpha_{sr}$, where $\alpha_{sr} < \alpha_s$ is the stall angle in the backward motion of the rudder blade. Then, it can be assumed that in this domain the normal force coefficient dependency $C_{Nr}(\alpha)$ can be represented as

$$C_{Nr}(\alpha) = C_{N0}(\pi - |\alpha|)\operatorname{sign}\alpha. \tag{39}$$

In the intermediate interval, i.e. when $|\alpha| \in (\alpha_s,\ \pi - \alpha_{sr})$, the normal force coefficient can be supposed to change, in the first approximation, linearly:

$$C_N(\alpha) = (a + b|\alpha|)\operatorname{sign}\alpha, \tag{40}$$

where the linear approximation coefficients are:

$$b = \frac{C_{N0}(\alpha_s) - C_{N0}(\alpha_{sr})}{\alpha_s + \alpha_{sr} - \pi}, \qquad a = C_{N0}(\alpha_s) - \alpha_s b. \tag{41}$$

5.4. Rudder inflow velocities and attack angles

The rudder attack angle is defined as

$$\alpha_R = \delta_R - \beta_R - \delta_{R0}, \tag{42}$$

where δ_R is the rudder deflection angle, β_R is the local drift angle, and δ_{R0} is the neutral (balancing) deflection angle. The attack angle must, however, be normalized to fall into the interval $[-\pi, \pi]$. In the case when $2\pi \geq |\alpha_R| > \pi$:

$$\alpha_R := \alpha_R - 2\pi \operatorname{sign}\alpha_R. \tag{43}$$

Let us consider the rudder geometric (i.e. not accounting for the hull and propeller influence) velocities u_R and v_R. Similar velocities for the propeller ahead of the rudder will be u_P and v_P. All these velocities generate the speed magnitudes $V_R = \sqrt{u_R^2 + v_R^2}$ and $V_P = \sqrt{u_P^2 + v_P^2}$, and the kinematic sidewash angles β_R and β_P defined in such a way that

$$u_R = V_R \cos\beta_R, \quad v_R = -V_R \sin\beta_R; \qquad u_P = V_P \cos\beta_P, \quad v_P = -V_P \sin\beta_P. \tag{44}$$

The next step is to link the stand-alone-rudder velocities u_R and v_R to the rudders apparent velocities behind the hull u_{RA} and v_{RA} connected similarly to V_{RA} and β_{RA}.

The longitudinal velocity is modified by the rudder wake fraction w_R:

$$u_{RA} = u_R(1 - w_R) = u(1 - w_R), \tag{45}$$

where, similarly to the propeller,

$$w_R = w_{R0} e^{K_1 \beta_R^2}. \tag{46}$$

The last equation is the empiric formula introduced by Inoue et al. [19] with $K_1 = -4.0$ and $w_{R0} = 0.4$ (the latter value was recommended by Kose [30]) although both parameters can be adjusted. As with the propeller, the formula (46) gives reasonable estimate for any possible value of β_R.

The hull's influence on the transverse rudder velocity is formulated by Inoue et al. [19] directly in terms of the sidewash angle but this becomes inconvenient when applied to arbitrary manoeuvres. However, it can be relatively easily re-formulated in terms of the rudder transverse velocity as follows:

$$v_{RA} = \kappa_v(\bar{\beta}_R)\, v_R, \tag{47}$$

where the function $\kappa_v()$ is defined as:

$$\kappa_v(\beta) = \begin{cases} \min(K_2,\ K_3|\beta|) & \text{at } |\beta| < \beta_1, \\ a_v + b_v|\beta| & \text{at } |\beta| \in [\beta_1,\ \beta_2], \\ 1.0 & \text{at } |\beta| > \beta_2, \end{cases} \tag{48}$$

where $K_2 = 0.5$, $K_3 = 0.45$ and $a_v = 0.5 - b_v\beta_1$; $b_v = 0.5/(\beta_2 - \beta_1)$.

Assuming that the hull's influence vanishes at $|\beta| \geq \frac{\pi}{2}$, it is reasonable to set $\beta_1 = 1.3$ and $\beta_2 = \frac{\pi}{2}$.

The special sidewash angle $\bar{\beta}_R$ in Eq. (47) is restored in the standard way from u_R and $\bar{v}_R = v + \bar{k}x_R r$ where $\bar{k}$ is adjustable and Inoue et al. [19] recommend $\bar{k} = 2.0$ which is in agreement with the data presented by Kose [30]. Necessity of introducing this special sidewash angle is due to the fact that the hull's influence depends on the quasi-velocities v and r in a more complicated way than could have been obtained postulating its dependence on the geometric sidewash angle only. Introduction of separate straightening factors for the sway and yaw parts of the sidewash could be an alternative.

5.5. Influence of propeller slipstream

The approximate mathematical model for the propeller influence described below is based on the classic actuator disc theory. According to this theory, any propeller is represented as a thin disc of the area A_0 placed into the uniform flow with the velocity $\mathbf{v}_A$ directed along the normal to the disc. The disc is somehow generating a uniform jet whose axis is collinear with $\mathbf{v}_A$. In the present application, it can be assumed that $|\mathbf{v}_A| \equiv |u_{PA}|$ and then, as established in the actuator disc theory [32], the axial induced velocity at infinity is

$$w_{a\infty} = u_{PA}(\sqrt{1 + C_{TA}} - 1) \tag{49}$$

where the loading coefficient is

$$C_{TA} = \frac{2|T|}{\rho u_{PA}^2 A_0} \tag{50}$$

It follows from (49) that the total jet velocity at infinity behind the disc is

$$u_\infty = u_{PA} + w_{a\infty} = u_{PA}\sqrt{1 + C_{TA}} \tag{51}$$

The latter formula can be re-written in the following equivalent form which can be used also in the bollard regime:

$$u_\infty = \sqrt{u_{PA}^2 + w_{a0\infty}^2} \tag{52}$$

where

$$w_{a0\infty}^2 = \frac{2|T|}{\rho A_0} \tag{53}$$

is the squared infinity axial induced velocity in bollard regime.

The axial induced velocity is varying along the jet theoretically reaching its ultimate value at infinity behind the disc. Its value in the disc is $w_{a0} = (1/2)w_{a\infty}$. The sectional area of the jet is varying inversely to satisfy the continuity equation. Of course, in the real fluid the jet after certain region of contraction and acceleration will start to dissipate involving additional fluid but loosing its average velocity. However, the perfect fluid model still works adequately at all distances where the rudder can be located.

The longitudinal velocity of the part of the rudder inside the slipstream with respect to water is

$$u_{RP} = u_{PA} + w_a \tag{54}$$

where the axial induced velocity depends on the distance between the propeller and the rudder and can be represented as

$$w_a(\bar{x}) = \frac{1}{2}\kappa k_w(\bar{x}) w_{a\infty} \tag{55}$$

where κ is the empiric correction factor introduced by Kose [30] with the recommended value 0.68, and the distance factor

$$k_w(\bar{x}) = \left[\left(1 + \frac{\bar{x}}{\sqrt{1+\bar{x}^2}}\right)\kappa(T)\right] \operatorname{sign} T \tag{56}$$

where the relative signed distance from the propeller to the rudder

$$\bar{x} = \frac{2(x_P - x_R)}{D_P} \operatorname{sign} T \tag{57}$$

and

$$\kappa(T) = \begin{cases} 1 & \text{at } \bar{x}T \geq 0, \\ 0.7 & \text{at } \bar{x}T < 0 \end{cases} \tag{58}$$

Attention must be paid that the thus defined factor k_w is valid for any sign of the thrust although the propulsor works approximately as a disc of sinks from the side to which the thrust is directed while it produces a jet in the opposite direction. The coefficient κ is empiric.

The transverse component of the rudder-in-the-slipstream velocity is usually assumed to be the same as outside the slipstream i.e. $v_{RP} \equiv v_{RA}$. This definitely can be applied on the suction side of the actuator disc. However, even with strong sidewash, in the vicinity of the propeller disc the jet keeps its direction along the shaft axis as the transverse momentum is still not transmitted to it. Because of this, at $\bar{x}T > 0$ it is more reasonable to assume that $v_{RP} = (\bar{x}^2/a + \bar{x}^2)v_{RA}$, where a is an empiric constant.

Due to the jet's contraction, the slipstream-washed part of the rudder area A_{RP} depends on the distance $\bar{x}$. In general, it also depends on the relation between the rudder height and position and on how it is positioned with respect to the propeller axis. At the same time, the effective radius of the jet r_{RP} can be estimated as

$$r_{RP} = \frac{D_P}{2}\sqrt{\left|u_0/u_{RP}\right|}. \tag{59}$$

As has already been mentioned, the deflected rudder will also deflect the jet reducing its own attack angle. According to Söding [28] the corresponding factor k_d from Eq. (31) can be estimated as $k_d = \left|u_{RA}/u_{RP}\right|^f$, where $f = 2\left[2/(2 + d/b_R)\right]^8$, and $d = (\sqrt{\pi}/2)r_{RP}$.

6. Thruster forces

Many vessels are nowadays equipped with side tunnel thrusters to improve their low-speed controllability. These thrusters practically always work in the bollard regime which makes the thrust per se almost independent of the ship's motion but the interaction with the hull is rather complicated and affects significantly the effective sway force and yaw moment resulted from the thrusters' action.

The actual thrust T produced by a lateral jet thruster without account for the hull influence can be represented as $T = k_T T_0$, where $k_T \in [-1, 1]$ is the control parameter or the relative thrust (its value -1 corresponds to the maximum thrust to the portside, and $+1$—to the starboard), and T_0 is the maximum absolute thrust which is the main characteristic of the given thruster and is related to the thruster drive's power P_0 as [24]:

$$T_0 = c_0 P_0 \tag{60}$$

where the constant $c_0 = 0.15$ s/m accounts also for the hull pressure re-distribution.

The thus determined thrust T is effective on a deeply submerged thruster at zero surge (advance) speed of the ship. In a more general case, the sway force and the yaw moment from any single thruster should be calculated as follows:

$$Y_T = k_h(h_R)k_Y(\bar{u})T, \quad N_T = k_h(h_R)k_N(\bar{u})Tx_T, \tag{61}$$

where k_h is the submergence correction factor, $h_R = h/R$ is the relative submergence of the thruster, h is the submergence of its axis, R is the thruster's radius, k_Y, k_N are the longitudinal velocity correction factors, $\bar{u} = |u|/w_j$ is the absolute value of the relative longitudinal velocity of the ship, w_j is the effective jet velocity, x_T is the thruster's abscissa.

Data on the submergence correction factor accounting for the loss of the thruster's effective area and for the surface wavemaking can be found in [33] and it can be approximated as

$$k_h = \min(1.0, a_h + b_h h_R), \tag{62}$$

where $a_h = 1/3$, $b_h = 17/30$. This factor does not account for aeration which can result in more drastic fall of the thrust but which is usually avoided in normal operation.

As to the velocity correction factors, they also depend on the thruster's location: near the stern or near the bow. Experimental data on k_Y for only the bow thruster at ahead ship speed belonging to Chislett and Bjørheden are presented by Faltinsen [33]. Brix [24] provides data for both bow and stern thrusters in ahead and astern speed but as functions of the dimensional velocity u. The value of the jet velocity w_j at those tests is not given explicitly but a remark about the properties of the correction factors made possible approximate restoration of w_j. In general, the jet velocity can be found as

$$w_j = \sqrt{\frac{|T|}{\rho A_0}} \tag{63}$$

where A_0 is the thruster's sectional area.

Then, Brix' data were approximated with second- or third-degree algebraic polynomials $a + b\bar{u} + c\bar{u}^2 + d\bar{u}^3$ separately for each case and safely continued outside the tested region with constant values although typically experimental data show (further) recuperation of the thrust. Values of the approximation coefficients are given in Tables 1 and 2.

In addition, the Chislett and Bjørheden data clearly show a small interval of constant values equal to unity for $|\bar{u}| < 0.12$. This is also justified by the process' physics as at small relative longitudinal speed no jet attachment or pressure re-distribution can occur. Unfortunately, the Brix data were obtained with a too large step and could not show this effect. So, it was decided to add the point (0.12, 1.0) to all Brix data. The resulting approximated responses together with the experimental data borrowed from Brix [24] and, in one case, Faltinsen [33] are shown in Figs. 4 and 5 where the absolute value of the relative longitudinal velocity is shown on the horizontal axes.

7. Aerodynamic forces

The aerodynamic forces can be represented as

$$\begin{aligned} X_A &= C_X(\beta_A, \xi_C, \eta_C)\frac{\rho_A V_A^2}{2}A_L, \\ Y_A &= C_Y(\beta_A, \xi_C, \eta_C)\frac{\rho_A V_A^2}{2}A_L, \\ N_A &= C_N(\beta_A, \xi_C, \eta_C)\frac{\rho_A V_A^2}{2}A_L L_{OA}, \end{aligned} \tag{64}$$

Table 1
Approximation coefficients for $k_Y(\tilde{u})$.

Thruster	u	a	b	c	d
Bow	>0	1.236133984568	−2.466381997565	1.621751193502	0.0
	<0	1.110973606193	−1.261200467681	0.9375221889657	0.0
Stern	>0	1.319106928965	−3.302007109009	3.075565631253	0.0
	<0	1.289253261375	−2.540634413509	1.610802566528	0.0

Table 2
Approximation coefficients for $k_N(\tilde{u})$.

Thruster	u	a	b	c	d
Bow	>0	1.334253478	−3.534640537	6.647727158	−3.66998672
	<0	1.121478745	−1.610981216	0.6918614180	0.0
Stern	>0	1.172907048	−1.965410978	2.054377528	0.0
	<0	1.135322201	−1.349292142	1.529502839	0.0

where $C_{X,Y,N}$ are the force/moment aerodynamic coefficients, ρ_A is the air density, A_L is the ship's lateral area, L_{OA} is the ship's length overall.

The aerodynamic coefficients are shown here as dependent on the ship's position. This makes sense when a non-homogenous wind field, as for instance, behind some obstacle, is considered. At present, data on aerodynamic characteristics of the ship hulls in non-homogenous wind are practically absent and then the coefficients will only depend on the air drift angle.

Independence of the aerodynamic forces on the angular velocity of yaw is commonly acknowledged but it is not so evident and deserves explanation. Assuming, however, in the case of a homogenous wind, that this dependence exists and taking into account Eqs. (5), (8) and (9) it is possible establish a complete list of arguments for any aerodynamic coefficient and to expand it into a multivariate Fourier series (here: with respect to the zero point, up to the first-order terms and for only sway force for simplicity):

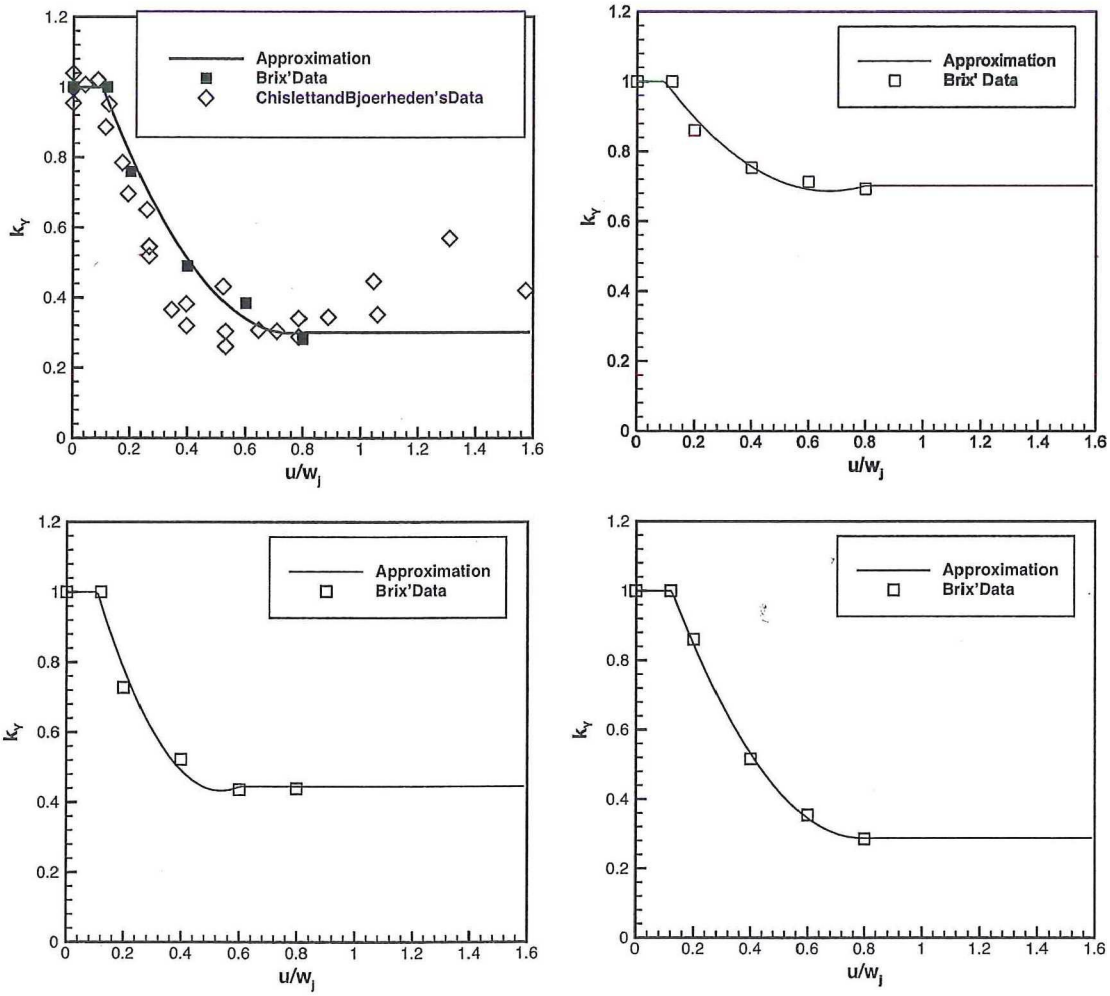

Fig. 4. Velocity correction factor for the sway force: upper row—bow thruster, lower row—stern thruster; left—ahead motion, right—astern motion.

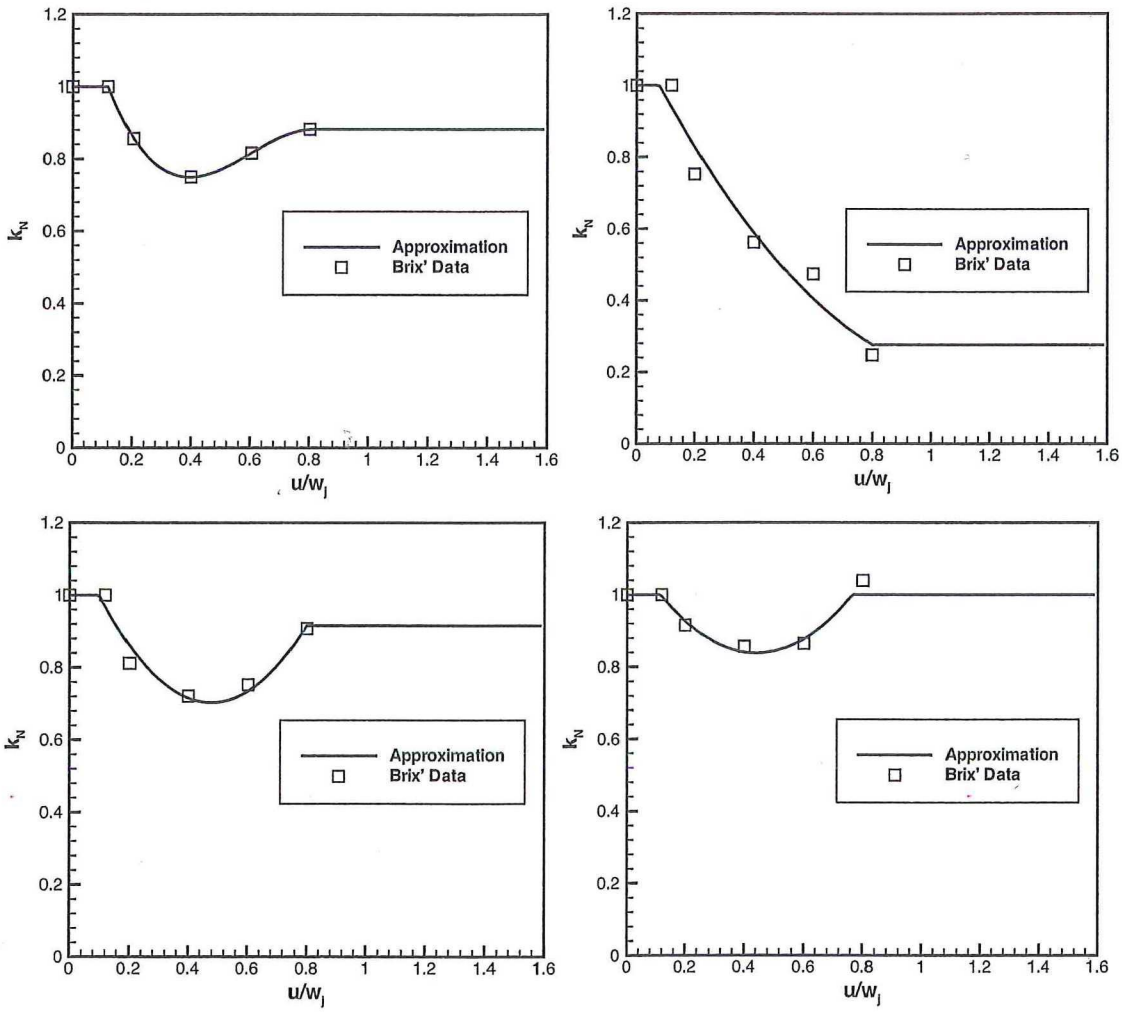

Fig. 5. Velocity correction factor for the yaw moment: upper row—bow thruster, lower row—stern thruster; left—ahead motion, right—astern motion.

$$C_Y(v', r', \chi_w, \psi) = C_Y^v v' + C_Y^r r' + C_Y^\chi \chi_w + C_Y^\psi \psi + \cdots \tag{65}$$

Here every term containing v' or r' has a hydrodynamic counterpart and, for instance, the hydrodynamic term $X_r'' r'$ must be compared with $(\rho_A A_L V_A^2 / \rho L T V^2) C_Y^r r'$. It is obvious that due to the very small air/water density ratio the latter is much smaller than the former even with large wind areas and velocities and thus can always be neglected. However, terms containing only variables χ_w and ψ do not have hydrodynamic counterparts at all and their presence explains why even a not very strong wind can change sensibly behaviour of the ship. But it is then also evident that this influence is completely accounted for through dependence of aerodynamic forces on the air drift angle β_A.

The aerodynamic coefficients C_X, C_Y and C_N are either determined experimentally (appropriate numerical tests are also possible) or estimated with the help of experiment-based databases and regressions. For the vessel in concern dedicated wind-tunnel tests were carried out and the obtained data were used in simulations presented in this paper. Description and analysis of the aerodynamic experiment are described in [44].

8. Additional components of the ship's mathematical model

Besides the main kinematic and dynamic equations of motion, any more or less complete manoeuvring mathematical model must include additional components describing some aspects of "internal" ship dynamics which are relevant for an adequate description of the manoeuvring motion. In the present consideration, these are sub-models for the propeller–shaft–gear–engine dynamics, dynamics of the main steam valve (in the case of a steam turbine as main engine), steering gear dynamics, and dynamics of the thruster's drive. The last three components are not always important and their presence does not influence heavily the observed behaviour of the ship but makes the response smoother which provides better feeling to the operator and can be important, for instance, in the sliding control mode.

8.1. Torque equation and main engine dynamics

Response of the dynamic system composed of the rotating propeller, shaft, main (propulsion) engine, and of the reduction gear, when present, is described by the following differential equation:

$$2\pi I_{pp} \dot{n} = Q_E(n, \kappa_V) + Q_P(n, u) + Q_F(n), \tag{68}$$

where I_{pp} is the effective rotational moment of inertia which includes the proper and added moments of inertia of the propeller, that of the shaft, and the transformed (to the propeller rotation frequency n) moment of inertia of the gear and engine; Q_E is the engine torque; κ_V is the governing parameter (like the main steam valve's opening for the turbine or the fuel rate setting for the diesel engine); Q_F is the friction torque which in most cases can be assumed as

$Q_F = -Q_{F0}\,\mathrm{sign}\, n$, where Q_{F0} is a constant depending on the specific type of the propulsion plant.

The function $Q_E()$ depends on the type of the engine and will be described here for the steam turbine serving as main engine on the LNG carrier *Galea* considered later as example.

For the purpose of the present study it was sufficient to recode the algorithm used by Sutulo and Yegorov [34] in the core model developed for a submarine manoeuvring simulator. The turbine's model is based on the common assumption about linear decay of the turbine's torque from its brake (zero rpm) value $Q_0(\kappa_V)$ to zero at the free run with the zero torque and the rotation frequency n_0. The allowed maximum rotating frequency n_m is, however, limited by the regulator. The brake moment Q_0 depends on the steam flow and the relative valve opening $\kappa_V \in [-1, +1]$.

As the power and torque of any turbine is, as a rule, reduced in the astern run, the constants in the following mathematical description will be appended by an additional subscript + or −. Hence,

$$Q_E = \begin{cases} Q_0(1 - n/n_0) & \text{at} \quad n \in [-n_{m-}, n_{m+}] \\ 0 & \text{otherwise,} \end{cases} \tag{69}$$

$$Q_0 = \begin{cases} Q_{0+}\kappa_V & \text{at} \quad \kappa_V \geq 0, \\ Q_{0-}\kappa_V & \text{at} \quad \kappa_V < 0; \end{cases} \qquad n_0 = \begin{cases} n_{0+}\kappa_V & \text{at} \quad \kappa_V \geq 0, \\ n_{0-}\kappa_V & \text{at} \quad \kappa_V < 0. \end{cases} \tag{70}$$

The maximum permitted rotation frequency n_{m+} is close to the design (specification) turbine speed n_d which is typically known together with the design rating. If the zero speed torque Q_{0+} is not available, it can be approximately estimated using typical decline of the turbine's torque characteristic.

The mentioned submarine turbine model was developed in contact with the customer who requested reproduction of a certain time lag not only in settling the ordered rotation frequency but also in the steam valve's opening settling. This was modelled by a simple valve dynamics equation:

$$\dot{\kappa}_V = \begin{cases} \lambda_V\,\mathrm{sign}(n^* - n) & \text{at} \quad |n^* - n| \geq \varepsilon_n \\ 0 & \text{at} \quad |n^* - n| < \varepsilon_n \end{cases} \tag{71}$$

where λ_V is the constant valve opening rate, and ε_n is the width of the dead zone for the rpm governor, n^* is the ordered rotation frequency.

8.2. Steering gear and thruster dynamics

It was assumed that dynamics of the rudder and of the side thruster can be described with similar models based on the first-order aperiodic plants augmented with some schematic nonlinearities.

The model for the steering gear is described in terms of the actual rudder angle δ_R and of the rudder order δ^*. Nonlinearities include the rudder angle saturation $|\delta_R| \leq \delta_m$, the rudder rate saturation $|\dot{\delta}_R| \leq \varepsilon_m$, and the non-sensitivity dead band of width δ_0. Then, mathematically, the steering gear is described by the ordinary differential equation:

$$\dot{\delta}_R = \begin{cases} \min\left[\frac{1}{T_R}(|\delta^{**} - \delta_R| - \delta_0), \varepsilon_m\right] \cdot \mathrm{sign}(\delta^{**} - \delta_R) & \text{at} \quad \mathbf{L} = \text{false}, \\ 0 & \text{at} \quad \mathbf{L} = \text{true}, \end{cases} \tag{72}$$

where **L** is the Boolean variable defined by

$$\mathbf{L} = (|\delta^{**} - \delta_R| < \delta_0) \vee [(|\delta_R| \geq \delta_m) \wedge (\mathrm{sign}(\delta^{**} - \delta_R) = \mathrm{sign}\,\delta_R)] \tag{73}$$

T_R is the time lag of the gear, and

$$\delta^{**} = \begin{cases} \delta^* & \text{at} \quad |\delta^*| \leq \delta_m, \\ (\delta_m + \delta_0)\mathrm{sign}\,\delta^* & \text{at} \quad |\delta^*| > \delta_m \end{cases} \tag{74}$$

is an auxiliary variable necessary to execute helms at ultimate angles and to prevent the winding up.

The adopted model for thruster drive is quite similar but written in terms of the actual relative thrust k_T and ordered relative thrust k_T^*.

9. Simple mathematical model for tugs

A fully consistent mathematical model for tug-assisted motion of a ship must consider combined manoeuvring of several (at least two) vessels connected with the towlines or having a close contact (when a tug works in the pushing mode). If these lines are long enough, their dynamics must be also taken into account. However, to make reasonable estimates of manoeuvring capabilities of tug-assisted ships, a much simpler concept of ideal tugs or *quasi-tugs* can be exploited (the latter terms explains the subscript Q associated here with the tug action).

This concept was inspired by the quasi-tug implementation in manned physical ship models (length up to 12 m) used in the Ship Handling Research and Training Centre in Iława, Poland. On these models, the same lateral thrusters were used to simulate the tug action but a constant time lag was introduced to reproduce the natural delay in changing the towing/pushing force' direction. In mathematical modelling, it is possible to implement a somewhat more sophisticated model with arbitrary thrust direction. Such kinds of tug models are known as vector tugs [35].

Each quasi-tug is characterized by the following parameters:

- maximum available effective thrust T_{Qm};
- speed V_Q at which the tug is operating at zero tension of the towline i.e. when the tug is re-positioned to apply the thrust in a different direction;
- the body-fixed co-ordinates x_Q, y_Q, z_Q of the point on the assisted ship to which the towline is fixed;
- the towline's length s.

Besides that, the following two controlling variables are involved:

- the relative ordered thrust τ;
- the towline direction with respect to the assisted ship's centreplane described by the towline angle $\gamma \in [-\pi, \pi]$ ($\gamma > 0$ when the towline stays on the starboard side; γ^* is the ordered towline direction).

Then, if at the moment t the control pair $(\tau(t), \gamma^*(t))$ is applied, this will result in the following action:

$$T_e(t') = \begin{cases} 0 & \text{at} \quad t' \in (t, t + T_{lag}) \\ \tau(t')T_{Qm} & \text{at} \quad t' \geq t + T_{lag} \end{cases}, \qquad \gamma(t') = \gamma^*(t) \quad \text{at} \quad t' > t, \tag{75}$$

where the thrust application lag is

$$T_{lag} = \frac{\pi s|\gamma^*(t) - \gamma(t)|}{V}. \tag{76}$$

The latter formula follows immediately from the assumption that in order to change the tow force direction, the tug travels along the circular arc of radius s with its constant re-position velocity V until the new direction of the towline is reached. Of course, the difference in the numerator must be found within the special

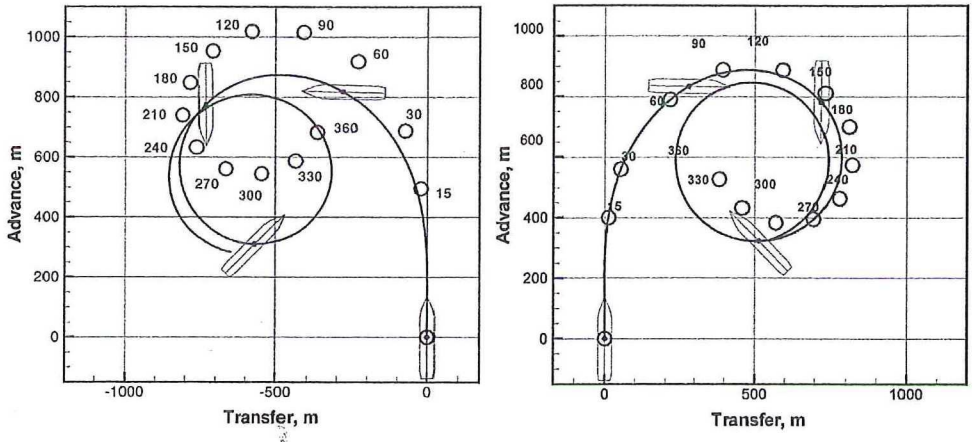

Fig. 6. Ship trajectories in tight turns: lines and images—simulation, larger filled circles—sea trials; numbers near the symbols indicate the heading change in trials.

Table 3
Main particulars and other parameters of the LNG carrier *Galea*.

Particular or parameter	Dimension	Numerical value	Remark
Length between PP	m	276	
Length overall	m	290	
Breadth	m	46	
Design draught	m	11.405	
Mean draught on trials	m	9.69	
Trim on trials	m	0.08	By the stern
Hydrodynamic reference area, *LT*	m^2	3148	
Design displacement	m^3	102,440	
Displacement on trials	m^3	84,035	
Maximum speed on trials	kn	19.84	
Engine's MCR	kW	21,320	Steam turbine
Engine's nominal speed	rpm	81	
Propeller's diameter	m	8.8	
Propeller's pitch	m	7.577	FPP
Number of blades		4	
Propeller's abscissa	m	−132.5	Estimated
Propeller's applicate	m	6.86	Estimated
Shaft vertical angle	deg	3.5	Estimated
Centre of mass' abscissa	m	3.08	
Waterplane centroid's abscissa	m	−1.705	
Elevation of the centre of buoyancy above the base plane, *KC*	m	6.09	
Transverse metacentre's elevation	m	22.34	
Block coefficient		0.7075	
Full rudder area	m^2	79.2	Estimated
Movable rudder area	m^2	60.6	Estimated
Horn's area	m^2	18.6	Estimated
Rudder's height	m	10.7	Estimated
Rudder root's chord	m	8.1	Estimated
Rudder tip's chord	m	6.7	Estimated
Rudder mean chord	m	7.4	Estimated
Horn's height	m	6.1	Estimated
Horn's chord	m	3.05	Estimated
Rudder's abscissa	m	−138.0	Estimated
Rudder' applicate	m	5.53	Estimated
Rudder' maximum deflection angle	deg	35	
Rudder' maximum deflection rate	deg/s	2.6	
Bow side thruster's diameter	m	1.8	Estimated
Bow side thruster's abscissa	m	123.2	Estimated
Bow side thruster's applicate	m	6.58	Estimated
Bow side thruster's maximum effective thrust	kN	230	Estimated
Aerodynamic lateral area	m^2	6500	Estimated
Abscissa of lateral area's centroid	m	0	Estimated
Aerodynamic transverse area	m^2	650	Estimated
Turning circle advance as measured on trials	m	1025/897	Portside/ starboard
Tactical diameter as measured on trials	m	807/826	Portside/ starboard

arithmetic i.e. in such a way that the result do not exceed π which corresponds to the shortest travel length. For instance, if $\gamma^* = -160°$ and $\gamma = +170°$ then: $|\gamma^* - \gamma| = 30°$. Assuming that the towline is long enough to make possible neglect of forces and moments acting in the vertical planes, the tug forces and moments in the body axes will be:

$$X_Q = T_e \cos\gamma, \quad Y_Q = T_e \sin\gamma, \quad N_Q = -X_Q y_Q + Y_Q x_Q, \tag{77}$$

where x_Q, y_Q are the co-ordinates of the towline fixation point.

10. Examples of simulation and model validation

The shuttle LNG tanker *Galea*, whose data are given in Table 3, was chosen as the simulation object.

This is a single-screw single-rudder ship driven with a steam turbine and equipped with a single bow thruster.

10.1. Turning circles

Turning circles with full helm (35°) have been simulated first. Trajectories for the starboard and port turns are shown with solid lines and ship images at characteristic positions in Fig. 6 where are also plotted results of sea trials from Galea [36]. The trials for both starboard and port turn were conducted with the wind 5 Beaufort and 135° direction (backstay) with respect to the approach course and so were performed the simulations. The agreement in trajectory for the starboard turn looks good although the simulated turn is performed somewhat faster and, apparently, with much larger drift angles. The latter, however, correspond to those expected on a ship with high turning ability while the drift observed during the trials looks, on the contrary, too small. The agreement is worse for the port turn: the tactical diameter still corresponds well but the advance remains underestimated. However, the trials show higher influence of the wind direction than could be expected from this ship at moderate wind, and could result from some unrecorded gust.

10.2. Crash stop

The stopping manoeuvre was simulated with the rudder amidship and in absence of wind with initial ahead speed 19kn which corresponded to the described trial conditions. Time histories for the velocity of surge u (this velocity is typically measured by most of ship logs) and for the heading angle increment are presented in Fig. 7. The agreement looks very good for the velocity but somewhat worse for the heading.

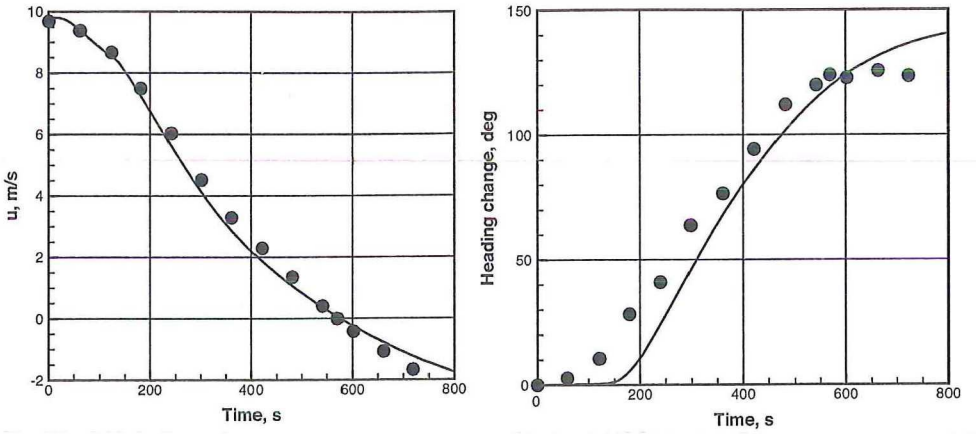

Fig. 7. Time histories in crash stop: lines—simulation, circles—sea trials; left—velocity of surge, right—heading.

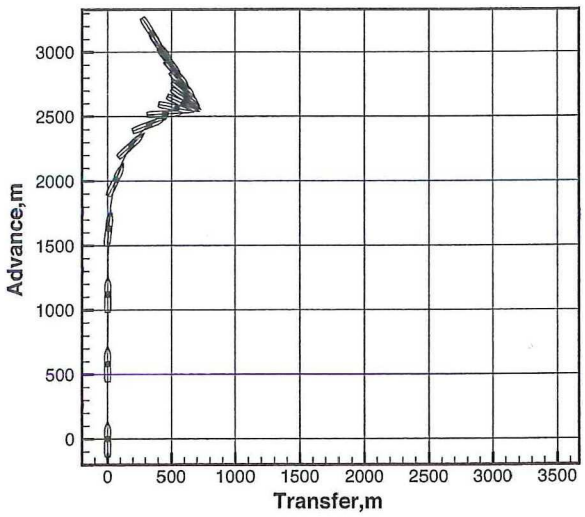

Fig. 8. Simulated trajectory in crash stop: interval between ship images—60 s.

As result, the final transfer of the ship was underpredicted: 1150 m in trials but only 700 m in simulation. At the same time, the head reach was slightly overpredicted: 2600 m versus 2400 m measured. The most likely these differences are due to a too crude modelling of the Hovgaard force although qualitatively the behaviour of the ship was captured. The ship's trajectory in crash stop (only simulated) is given in Fig. 8. Observed data on the heading change show practical absence of ship turning in backing motion after the stop which, however should not be expected as the Hovgaard effect continues to be present.

10.3. Lateral thruster turning

During the trials, turning with the bow thruster was performed from the stopped position to the starboard and port sides. The wind was 9 m/s, strictly bow wind for the port turn and 10° from starboard for the starboard turn. In the both cases, the thruster was producing maximum thrust. Time histories, both simulated and measured in full-scale trials are presented in Fig. 9 and the corresponding trajectories (only simulated)—in Fig. 10. Some differences in the behaviour in starboard and port turns are explained by different initial wind direction but also by a certain aerodynamic asymmetry of the LNG carrier [44].

10.4. Spiral manoeuvre

This manoeuvre was not performed in sea trials likely due to its increased time consumption. However, it was simulated, and not only using the developed mathematical model as described above and as used for all remaining moderate and hard manoeuvres, but also with modifications in the rudder and hull sub models. Namely, the developed 4-quadrant rudder model was substituted with the model recommended by Ogawa et al. [37], and the generalized mathematical model described in the present paper was

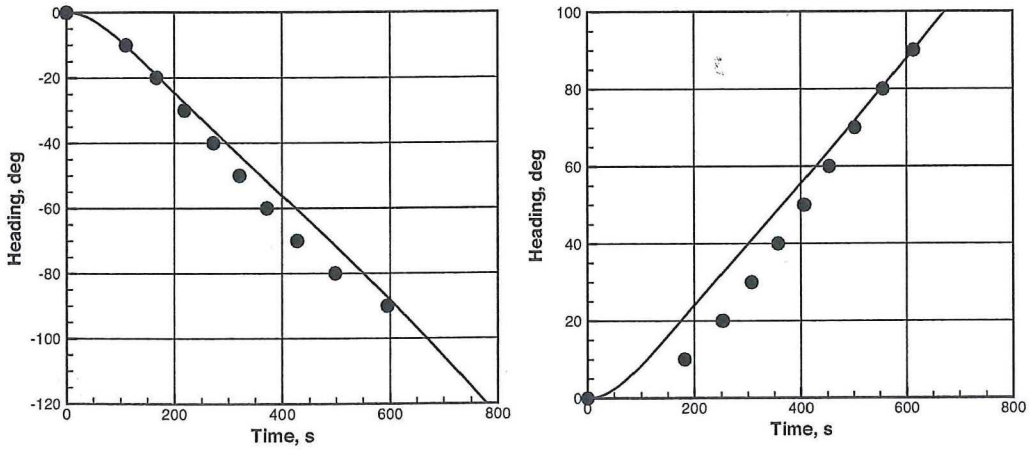

Fig. 9. Time histories in turns with the bow lateral thruster: line—simulation, symbols—trials.

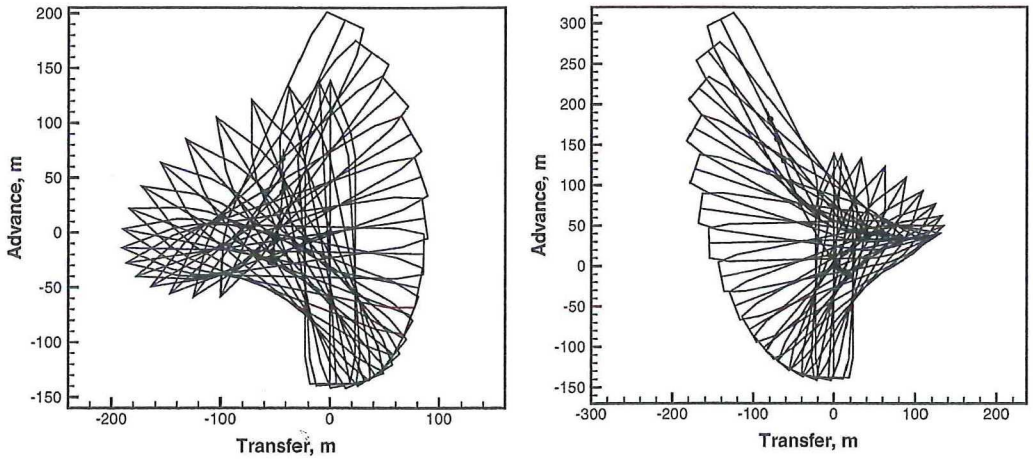

Fig. 10. Trajectories in turns with the bow lateral thruster: interval between ship images—60 s.

replaced with the original Inoue model. All spiral curves are presented in Fig. 11. It can be seen that the ship is detected as slightly directionally unstable independently of the model's modification. In all the cases, the half-height of the hysteresis loop is 0.15 and the half width is 0.75° i.e. very small. Loops of this width are very difficult to detect during the sea trials when the ship's response is masked with random errors.

However, at larger rudder angles different models produce different response. First, it must be noted that the main model (all 4-quadrant) gives the best agreement with sea trials (see results for the turning manoeuvre) at large rudder angles. The classic model (Inoue's hull and Ogawa's rudder) somewhat underestimates the turning ability but produces more expectable estimates for the dimensionless abscissa of the pivot point $x'_p = -v'/r'$ which means reduced values of the drift angle. Two other combinations resulted in worse predictions: the new rudder model combined with Inoue's polynomial hull model lead to substantial overestimation of the turning ability while Ogawa's rudder

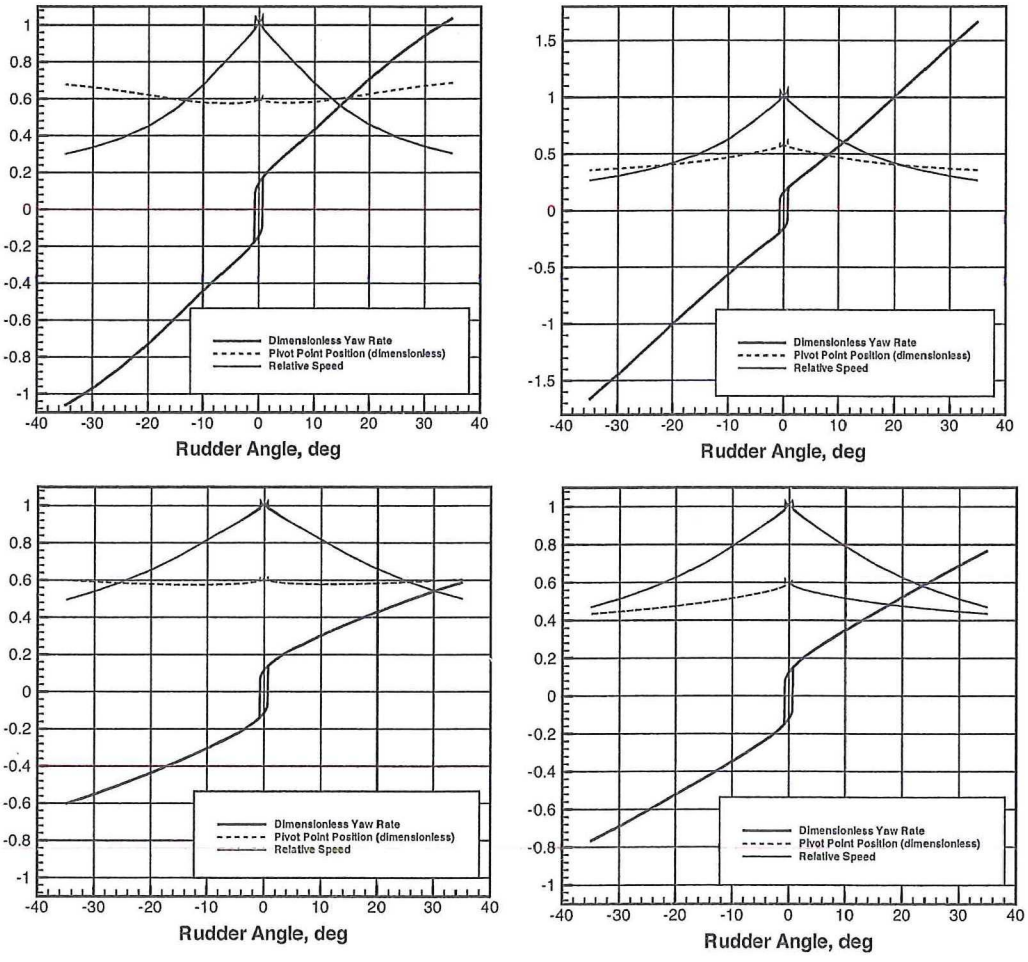

Fig. 11. Spiral curves: top—generalized 4-quadrant rudder model, bottom—Ogawa's rudder model; left—generalized 4-quadrant hull model, right—Inoue's hull model.

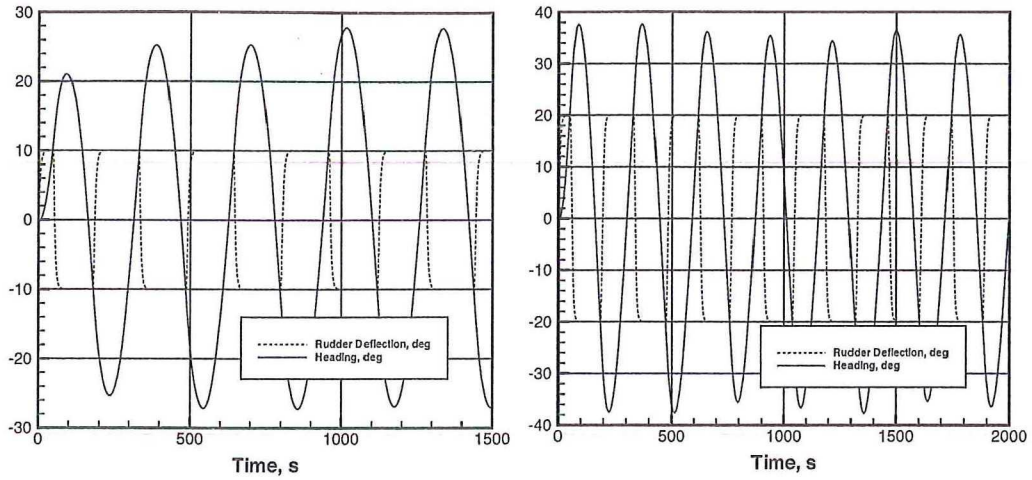

Fig. 12. Time histories in the zigzag manoeuvre: left—10°–10°, right—20°–20°

Table 4
Overshoot values.

Zigzag	Overshoot	Value (deg)	IMO standard
10°–10°	1st	21	19
	2nd	27	38.5
20°–20°	1st	37.5	25
	2nd	37.4	–

model combined with the 4-quadrant hull model underestimates it.

10.5. Zigzag manoeuvre

Standard zigzags 10°–10° and 20°–20° at 19kn approach speed have been simulated. The most relevant time histories $\delta_R(t)$ and $\psi(t)$ are exposed in Fig. 12. Captured values of the first and second overshoot angles are compared in Table 4. It can be seen that according to the simulated results, the vessel almost satisfies the IMO requirements for the 10°–10° zigzag but not for the zigzag 20° – 20° where the observed overshoot angle is 50% greater than allowed. The sea trials booklet [36] did not contain any evidence of performing zigzag tests and it remained unclear whether the vessel does really possess reduced course checking ability (could be expected from a ship with good turning ability and relatively small rudder) or the effect is mainly due to the mathematical model's peculiarities. The heading process in 20°–20° zigzag also reveals appearance of a low-amplitude subharmonic which is usually not observed in such simulations where a plain limiting cycle is expected. However, the mathematical model contains many sophisticated nonlinearities and possibility of such a behaviour cannot be ruled out.

10.6. Example of arbitrary manoeuvre

To check how the mathematical model behaves in more generalized situations when all or most controls are applied at the same time and the both environmental factors (current and wind) are in effect, a number of offline simulations have been performed. The trajectory and hull traces presented in Fig. 13 corresponds to the situation when the motion starts from the full stop although the ship is supposed to be driven by the 2 m/s current from the port to starboard. At $t=0$ the main propeller starts working dead slow astern with the rudder deflecting 35° to the starboard. Simultaneously, the bow thruster applies its full thrust to port and a tug is supposed to apply a 200 kN pull with the constant towline angle $\gamma=30°$ from

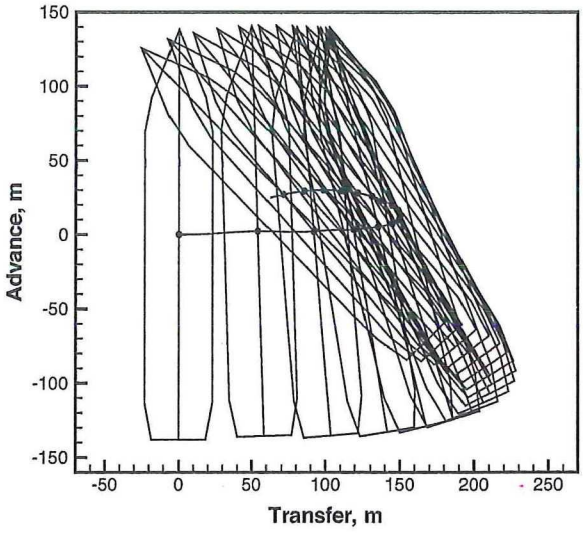

Fig. 13. Example of motion under combine influence of different factors: current 2 m/s from left to right, wind 10 m/s with the direction 135°, throttle 20% astern, thruster 100% to the portside, tug 100% at $\gamma=30°$; 60 s between the ship images.

the starboard. The wind direction is 135° which means backstay from the starboard. It can be seen that initially the ship's motion is caused exclusively by the current as this is the only permanent factor (i.e. not starting just at $t=0$). However, after approximately 3 min all the remaining factors inverse the situation and the vessel starts its turn to port with simultaneous slow return to the initial position.

11. Conclusions

A core mathematical model describing arbitrary 3DOF ship manoeuvring motions has been developed, coded and tested on a shuttle LNG carrier *Galea*. Although the model contains certain relatively novel elements assembled in a combination, it was primarily constructed as extension of a popular Inoue model for moderate manoeuvring and partly obtained on the basis of simple theories and empiric facts. No special model tests were carried out except for those related to the ship's aerodynamics.

Comparisons with full-scale data available for the full helm turning tests, crash stop tests and bow thruster turning demonstrated,

in general, good adequacy of the model achieved practically without special tuning.

Acknowledgment

The study was carried out within the project "SAFEOFFLOAD" (Safe Offloading from Floating LNG Platforms) funded by the European Commission through the GROWTH program under contract TST4-CT-2005-012560.

References

[1] Crane CL, Eda H, Landsburg A. Controllability. In: Lewis EV, editor. Principles of naval architecture, vol. 3. Jersey City, NJ: SNAME; 1989. p. 191–365.
[2] Sutulo S, Moreira L, Guedes Soares C. Mathematical models for ship path prediction in manoeuvring simulation systems. Ocean Eng 2002;29(1):1–19.
[3] Kijima K. Some studies on the prediction for ship manoeuvrability. In: Proceedings MARSIM'03. 2003. KN-3-1-10.
[4] Lewandowski EM. Dynamics of marine craft: maneuvering and seakeeping. Washington D. C.: World Scientific Publishing Co. Pte. Ltd.; 2004.
[5] Sutulo S, Guedes Soares C. An algorithm for optimized design of manoeuvring experiments. J Ship Res 2002;46(3):214–27.
[6] Sutulo S, Guedes Soares C. Development of a multifactor regression model of ship maneuvering forces based on optimized captive-model tests. J Ship Res 2006;50(4):311–33.
[7] Sutulo S, Guedes Soares C. An algorithm for offline identification of ship manoeuvring mathematical models after free-running tests. Ocean Eng 2014;79:10–25.
[8] Oltmann P, Sharma SD. Simulation of combined engine and rudder maneuvers using an improved model of hull–propeller–rudder interactions. In: Proceedings of the 15th ONR symposium on naval hydrodynamics. 1984. p. 1–24.
[9] Ankudinov VK, Miller Jr ER, Alman PR, Jakobsen BK. Ship maneuverability assessment in ship design—simulation concept. In: Proceedings of international conference on ship manoeuvrability—prediction and achievement. 1987.
[10] Kobayashi E, Asai S. A simulation study on ship manoeuvrability at low speeds. In: Proceedings of international conference on ship manoeuvrability—prediction and achievement, vol. 1, paper 10. 1987.
[11] Khattab O. Ship handling in harbours using real time simulation. In: Proceedings of international conference on ship manoeuvrability—prediction and achievement, vol. 1, paper 11. 1987.
[12] Burnay S, Ankudinov V. The prediction of hydrodynamic forces acting on the hull of a manoeuvring ship based upon a database of prediction methods. In: Proceedings of the international conference on marine simulation and ship maneuvering MARSIM'03. 2003. RC-2-1-12.
[13] Chislett MS. A generalized math model for manoeuvring. In: Proceedings of the international conference on marine simulation and ship manoeuvring MARSIM'96. 1996. p. 593–606.
[14] Sutulo S, Guedes Soares C. Mathematical models for simulation of manoeuvring performance of ships. In: Guedes Soares C, et al., editors. Marine technology and engineering. London: Taylor & Francis Group; 2011. p. 661–98.
[15] Barr RA. A review and comparison of ship maneuvering simulation methods. Trans SNAME 1993;101:609–35.
[16] Sutulo S, Guedes Soares C. An object-oriented manoeuvring simulation code for surface displacement ships. In: Guedes Soares C, Garbatov Y, Fonseca N, editors. Maritime transportation and exploitation of ocean and coastal resources. Leiden, The Netherlands: Taylor & Francis/Balkema; 2005. p. 287–94.
[17] Örnfelt M. Naval mission and task driven manoeuvrability requirements for naval ships. In: Proceedings of the 10th international conference on fast ship transportation, FAST 2009. 2009. p. 505–18.
[18] Sutulo SV. Extension of polynomial ship mathematical models to arbitrary manoeuvres. In: Proceedings of the international shipbuilding conference, section B. 1994. p. 291–8.
[19] Inoue S, Hirano M, Kijima K, Takashina J. A practical calculation method of ship maneuvering motion. Int Shipbuild Prog 1981;28:207–22.
[20] Van Mannen JD, Van Oossanen P. Resistance. In: Lewis EV, editor. Principles of naval architecture, vol. 1. Jersey City, NJ: SNAME; 1988. p. 1–126.
[21] Inoue S, Hirano M, Kijima K. Hydrodynamic derivatives on ship manoeuvring. Int Shipbuild Prog 1981;28:112–25.
[22] Kuiper G. The Wageningen propeller series. MARIN publication no. 92-001; 1992.
[23] Assenberg F, Sellmeijer R. Four-quadrant open water characteristics for B-series screw propellers. Fourier-like expansions in operational domain, Wageningen. Report no. 60482-1-MS; 1984 [in Dutch].
[24] Brix J. Manoeuvring technical manual. Hamburg: Seehafen Verlag; 1993.
[25] Anissimova NI, Sobolev GV. Experimental study of transverse force on a single-screw ship's hull in reversing regime. Trans Sci Soc Shipbuild Ind 1972;185:111–20 [in Russian].
[26] Ambrosovsky VM, Katz EB. Simulation of acceleration/deceleration maneuvers in navigation trainers problems. In: Proceedings international symposium on manoeuvrability of ships at slow speed. 1995. p. 119–32.
[27] Ogawa A, Kasai H. On the mathematical model of maneuvering motion. Int Shipbuild Prog 1978;25:306–19.
[28] Söding H. Prediction of ship steering capabilities. Schiffstechnik 1982;29:3–29.
[29] Söding H. Prediction of manoeuvring qualities in the design stage. Jahrbuch der Schiffbautechnischen Gesellschaft 1984;78:179–204 [in German].
[30] Kose K. On a new mathematical model of maneuvering motion of a ship and its applications. Int Shipbuild Prog 1982;29:205–20.
[31] Prishchemikhina TYu, Zlotin SE. Circular wind-tunnel tests of airfoils for prediction of four-quadrant characteristics of screw-propellers. In: Transactions of the USSR society of naval architects, issue 296: "tools and methods for full scale studies of seakeeping qualities of ships". Leningrad: Sudostroyeniye Publishing House; 1979. p. 55–60 [in Russian].
[32] Bertram V. Practical ship hydrodynamics. Oxford: Butterworth Heinemann; 2000.
[33] Faltinsen OM. Sea loads on ships and offshore structures. Cambridge, UK: Cambridge University Press; 1990.
[34] Sutulo SV, Yegorov SV. A submarine manoeuvring simulator as tool for expert and integrated control systems. In: Transactions of third international conference in commemoration of the 300th anniversary of creation of Russian fleet by Peter The Great (CRF-96), vol. 1. 1996. p. 525–39.
[35] Hensen H. Ship bridge simulators: a project handbook. London: The Nautical Institute; 1999.
[36] Galea.Galea: results of sea trials (hull part), drawing no. GCO-ZA0009F. 2002, 16 pp.
[37] Ogawa A, Hasegawa K, Yoshimura Y. Mathematical modeling of the ship's maneuvering. Nihon Zosen Gakkaishi (Techno Marine) 1980;616:565–76 [in Japanese].
[44] Wnęk A, Paço A, Zhou X-Q, Sutulo S, Guedes Soares C. Experimental study of aerodynamic loads on an LNG carrier and floating platform. Appl Ocean Res 2014 [in this issue].